Q_{EC} value and internal bremsstrahlung spectra of ^{179}Ta

M. M. Hindi,[1,*] B. O. Faircloth,[1] R. L. Kozub,[1] K. R. Czerwinski,[2,†] R.-M. Larimer,[2] E. B. Norman,[2] B. Sur,[2,‡] and I. Zlimen[2]

[1]*Physics Department, Tennessee Technological University, Cookeville, Tennessee 38505*

[2]*Nuclear Science Division, Lawrence Berkeley National Laboratory, Berkeley, California 94720*

(Received 27 December 2000; published 22 May 2001)

The total and $2p$ internal bremsstrahlung spectra accompanying the electron capture decay of ^{179}Ta have been measured in singles and in coincidence with L x rays, respectively. The intensity of the total spectrum was found to be (1.131 ± 0.027) times that predicted by the calculations of Surić *et al.*; the intensity of the $2p$ spectrum was found to be (1.097 ± 0.028) times those calculations. The disagreement with theory is thus much smaller than the factor of 1.5–2 previously reported for ^{193}Pt. The Q_{EC} value determined from the internal bremsstrahlung end point energy was found to be 105.61 ± 0.41 keV. An independent value for Q_{EC} of 109.3 ± 3.1 keV was determined by measuring the L to K capture ratio.

DOI: 10.1103/PhysRevC.63.065502 PACS number(s): 23.40.−s, 14.60.Pq, 21.10.Dr, 27.70.+q

I. INTRODUCTION

Electron capture is a weak interaction process in which a nucleus decays by capturing an atomic electron and ejecting an electron neutrino. A small fraction of such decays proceed radiatively, with the neutrino, atom, and emitted photon sharing the decay energy statistically. The produced radiation, which has a continuous energy spectrum, is known as internal bremsstrahlung (IB) and the decay process is referred to as internal bremsstrahlung electron capture (IBEC). The study of IBEC can yield information on the weak interaction, nuclear parameters, and atomic wave functions. Accurate isobaric atomic mass differences can also be deduced from the end-point energy of the IB spectrum. A thorough review of the theory and experimental status of IBEC up to 1977 is given by Bambynek *et al.* [1]. As pointed out in that review, while the main features of IBEC are generally understood, there is still a great need for experimental work to test the details of the theory. In particular, Bambynek *et al.* pointed out that precise measurements of normalized IB spectra are very much needed, as well as measurements of partial spectra that accompany the capture of electrons from specific atomic subshells.

Interest in IBEC decays was renewed after De Rújula's suggestion in 1981 [2] that the shape of the IB spectrum near the end point be used to search for neutrino mass. The best sensitivity is obtained for decays with low Q values, where the IB spectrum is dominated by capture from p orbitals and could be strongly enhanced by the presence of $p\rightarrow s$ poles in the electron propagator, if a decay with the right energy is found. Riisager *et al.* [3] carried out detailed measurements on the IBEC decay of ^{193}Pt to test De Rújula's extensions of the Martin-Glauber theory [4,5]. Although the calculations reproduced the measured shapes of the IB spectra, the magnitudes were off by factors of 1.5–2. The upper limit which Riisager *et al.* quoted on the mass of the electron neutrino is 500 eV, at the 90% confidence level. Springer, Bennett, and Baisden [6] measured the IBEC spectrum of ^{163}Ho and compared the data with a model similar to that used by Riisager *et al.* They quoted an upper limit on the mass of the electron neutrino of 225 eV, at the 95% confidence level, and concluded that improvements of this result would be severely limited by uncertainties in atomic interference effects.

The above limits on the mass of the electron neutrino are much higher than the corresponding limits of 5–10 eV [7] on the mass of the electron antineutrino and could certainly be improved upon, if, among other things, the uncertainties in the calculated IB spectra could be removed. Recently, Surić, Horvat, and Pisk [8] reformulated the relativistic theory of IBEC and developed a numerical code to calculate IBEC matrix elements. They included all relativistic and screening effects within an independent-particle approximation. They examined the case of ^{163}Ho and found a simpler structure of the total IBEC spectrum and a smaller interference suppression than predicted by the previous calculations [3,6]. Their calculation for ^{193}Pt, however, was still lower than the data by about a factor of 2.

To test the reformulation of Surić *et al.* of the IBEC theory, our group has compared their calculation with our measured IB spectrum of ^{125}I above the $1s$ end point [9,10] and our measured IB spectrum of ^{139}Ce [11]. It was found that the calculation reproduces the shape and relative intensity of the ^{125}I partial IB spectra to within the experimental error of a few percent. The measured intensity for ^{125}I was found to be 1.00 ± 0.12 [10,11] times the calculated intensity, and that for ^{139}Ce was found to be 1.070 ± 0.024 times the calculated intensity. While the ^{139}Ce work suggests that the calculation of Surić *et al.* does underestimate the intensity of the IB spectrum, it does so by only $7.0\pm2.4\%$, and not by the factor of 1.5–2 which is obtained for ^{193}Pt. To test if the deviation from the calculation of Surić *et al.* increases substantially as Z increases, we have measured the absolute intensity of the total and $2p$ IB spectra of ^{179}Ta. Three sets of measurements were made: (1) a set of singles measurements

*Present address: Celoxica Inc., 900 East Hamilton Ave., Suite 150, Campbell, CA 95008.

†Present address: Nuclear Engineering Department, Massachusetts Institute of Technology, Cambridge, MA 02139.

‡Present address: Chalk River Nuclear Laboratories, Chalk River, Ontario, Canada.

to obtain the total IB spectrum, (2) a set of L–x-ray–IB coincidence measurements to obtain the $2p$ IB partial spectrum, and (3) L to K capture ratio measurements to obtain a value for Q_{EC} independent of that determined from the IB end point.

II. EXPERIMENTAL PROCEDURES

A. Source preparation

The ^{179}Ta source was produced at the Lawrence Berkeley National Laboratory's 88-Inch Cyclotron via the ^{179}Hf$(p,n)^{179}$Ta and ^{180}Hf$(p,2n)^{179}$Ta reactions. Two pieces of natural hafnium, each 0.75 mm thick, were stacked together and bombarded for 17 h by a 5 μA beam of 20 MeV protons. After waiting for several months to let short-lived activities in the source decay away, the Ta was separated radiochemically from the hafnium target. The target was dissolved in a mixture of concentrated HF and HNO_3. Then an organic/aqueous separation of Ta was performed using methyl isobutyl ketone. The radiochemistry was repeated until the only observable activity was that due to ^{179}Ta. Approximately 7 months after the initial bombardment the source was shipped to Tennessee Technological University (TTU) in solution form. There it was evaporated onto a piece of Scotch tape and sealed with a similar piece. The initial activity of the sealed source was about 0.1 μCi. Another source was similarly produced 2 years later to continue with the investigations. The counting measurements described below were conducted at TTU.

B. IB measurements

1. Total IB spectrum

The total IB spectrum of ^{179}Ta was measured in singles using a well-shielded intrinsic planar Ge detector with a 16-mm diameter, 10-mm depth, and a 0.128-mm-thick Be window. An aluminum absorber with a thickness of $\approx$0.5 mm was placed in front of the detector to attenuate the Hf L x rays sufficiently so that their pileup with the Hf $K\beta$ x rays into the IB region was negligible. The ORTEC 572 amplifier had a 3-μs shaping time and was equipped with pileup rejection circuitry. The amplifier pulses were digitized using an ORTEC 916 PC-based multichannel analyzer (MCA) card. Spectra were saved to disk every 12 h.

Two sets of data were collected, one with the source as close as possible to the detector, thus producing a ''high count rate'' spectrum, and one with the source a few mm away from the detector, thus producing a ''low count rate'' spectrum. The primary reason for collecting data at different rates is to ensure that the procedure for subtracting (the rate-dependent) residual pileup was adequate. The ''high count rate'' data were collected for a total period of 17.83 days of live counting, at an average rate of 326.4 counts per second (cps). The ''low count rate'' data were collected for a total period of 25.00 days of live counting, at an average rate of 176.6 cps. A background spectrum totaling 22.70 days of live counting was also collected.

To verify that the yield in the IB region is due to higher energy γ rays, rather than due to a high-energy tail in the response function of the detector to the lower energy K x rays, we also collected a spectrum with the K x rays differentially attenuated. This was done by inserting a 1.2-mm-thick Cu absorber in front of the detector. The attenuated spectrum was collected for a period of 12.50 d, at an average count rate of 38.70 cps.

2. 2p IB spectrum

A separate set of coincidence experiments were conducted to measure the $2p$ IB spectrum. The spectrum was obtained from coincidences between L x rays and IB photons, recorded in the planar Ge detector described above and a coaxial Ge detector with a 43.5-mm diameter, 45.3-mm depth, a 3-mm crystal-to-endcap distance, and a 0.5-mm Be window. The detectors were placed face to face with the ^{179}Ta source sandwiched in between. Four sets of data were analyzed, three obtained with a weaker source prepared in 1990 and one obtained with a stronger source prepared in 1992. The measurements with the 1990 source were conducted in 1991, while those with the 1992 source were conducted in 1996. The first experiments were conducted without any absorbers, thus allowing two sets of L-IB coincidence spectra to be obtained, one with the L's detected in the planar detector and the other with L's detected in the coaxial detector. However, we found that there was residual pileup of L and $K\alpha$ x rays. To eliminate this pileup peak, we conducted the remaining measurements with an aluminum absorber between the source and the coaxial detector. The last two sets of data (one from 1991, the other from 1996) were obtained with this absorber in place.

All data were recorded event by event on magnetic tape. In addition to recording the two energy signals, two timing signals were recorded for each detector, one obtained from a low threshold on the leading edge module and one from a high threshold. The time difference between the two thresholds gives a measure of the risetime of each pulse. A further reduction in pileup can be obtained by gating on a two-dimensional (2D) plot of the rise time versus energy for each detector, as explained in Ref. [12].

C. L-to-K capture ratio measurements

A separate set of experiments was conducted to measure the L to K capture ratio for ^{179}Ta. From this set one can obtain a value for Q_{EC} independent of that determined from the IB end point. To our knowledge our technique is novel and does not require knowledge of the efficiency of any detector for L x rays. To motivate the setup we used for this measurement we give here a brief explanation of the principle of the measurement; the detailed expressions relating the measured rates to the Q value are given in Sec. III B. Consider an experiment in which L x rays are detected in one detector and K x rays in another, with both coincidence and singles rates being recorded. The number of L-$K\alpha$ coincidences is proportional to (among other things) the efficiency of the L x-ray detector and the K-capture probability P_K. The number of L x rays in *anticoincidence* with the K x-ray detector is again proportional to the efficiency of the L x-ray detector and a sum of two terms, one proportional to the

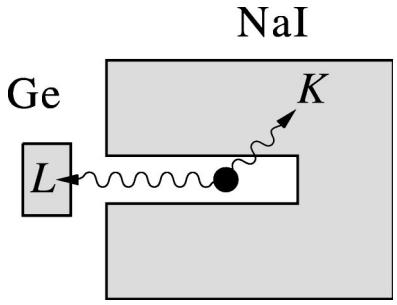

FIG. 1. Schematic diagram of the detector setup used in the L-to-K capture ratio measurements. K x rays emitted by the ^{179}Ta source were detected by the well-type NaI detector, while L x rays were detected by the planar Ge detector.

L-capture probability P_L and the other to P_K, to account for the fraction of K x rays that escape vetoing. The coincidence-to-anticoincidence ratio is therefore independent of the efficiency of the L x-ray detector and can be used to determine P_L/P_K, and hence Q_{EC}, provided one knows the absolute vetoing efficiency. The vetoing efficiency is much easier to determine than the efficiency for L x rays, since it involves measuring the efficiency for $K\alpha$ x rays at an energy of $\sim$55 keV, around which there are lines from calibration sources, such as ^{133}Ba, and for which the difference in self-absorption between the ^{179}Ta source and the calibration source is negligible. Most conventional methods would have required knowledge of the efficiency for L x rays; the energy of these ($\sim$10 keV) is low enough for self-absorption, and its variation between a calibration source and the ^{179}Ta source, to potentially become a major source of systematic uncertainty.

To maximize the sensitivity of the anticoincidence yield to P_L one has to maximize the vetoing efficiency for $K\alpha$ x rays, i.e., make the efficiency of the K x-ray detector as large as possible. To that end, we used a well-type NaI crystal for our K x-ray detector. The cylindrical crystal had a diameter of 5.7 cm and a height of 6.3 cm; the coaxial well had a diameter of 1.5 cm and a depth of 3.9 cm. The ^{179}Ta source was placed at a depth of 2.0 cm into the well. The L x rays were detected in the planar Ge detector described above. The Ge detector was placed facing the NaI detector, as shown schematically in Fig. 1.

Coincidence and singles events were recorded event by event on magnetic tape for later analysis. Measurements were performed on both the 1990 and 1992 sources. The rate of emission of K x rays by each source was determined in separate singles measurements, using the planar Ge detector, after determining its efficiency curve using calibrated sources of ^{133}Ba, ^{109}Cd, and ^{57}Co. Dead-time corrections were made using a precision 60 Hz pulser.

III. DATA ANALYSIS AND RESULTS

A. IB spectra

1. Total IB spectrum

The net IB spectra were produced by subtracting the contribution of background and of residual pileup from the raw spectra. The background was subtracted by normalizing the measured background spectrum to the raw ^{179}Ta spectrum in the energy region 153–295 keV. This way of normalizing the background spectrum agreed with a normalization based on the ratio of the live times (as measured by the MCA card) to within 2%. This small difference between the two normalization parameters is well within the accuracy of the live-time calculation of the MCA; this later accuracy was checked by a comparison of the live-time reported by the MCA with that obtained using the precision 60 Hz pulser during the collection of some calibration spectra. (The pulser was *not* used during the collection of the total IB and background spectra used in this analysis, and thus a pulser-based calculation of the live time was not possible.) The normalized background spectra for the ''high count rate'' and ''low count rate'' data are shown in Figs. 2 and 3, respectively. The background spectrum shows a slight ^{179}Ta contamination, but this is too small ($\approx 5\times10^{-5}$ of the raw ^{179}Ta spectrum) to be of any significance. The pileup spectrum was calculated using the Monte Carlo simulation procedure described in Ref. [11]. The intensity of the pileup spectrum was obtained by normalizing the Monte Carlo-simulated spectrum to the background-subtracted ^{179}Ta spectrum in the energy interval 108–130 keV. The normalized pileup spectra for the ''high count rate'' and ''low count rate'' data are shown in Figs. 2 and 3, respectively.

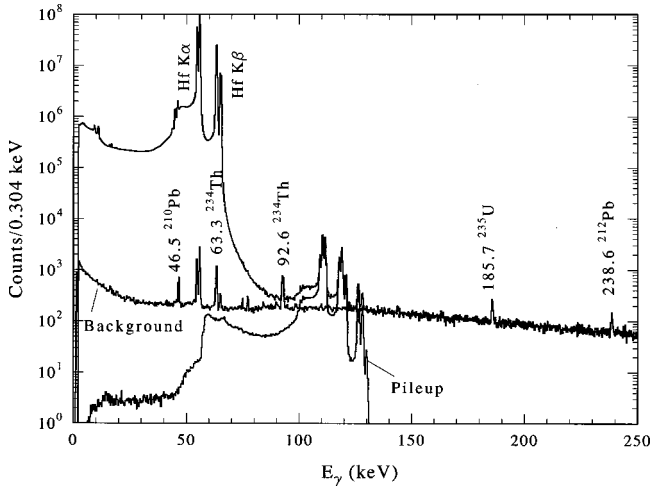

FIG. 2. The raw ''high count rate'' γ-ray spectrum of ^{179}Ta, together with normalized background and pileup spectra. The ^{179}Ta spectrum represents 17.83 days of counting at an average count rate of 326.4 counts per s. The background spectrum represents a total of 22.70 days of counting.

The net IB yield for the ''high count rate'' data, divided by the number of K captures and by the width of the energy bin (0.304 keV), is shown in Fig. 4. The number of K captures was deduced from the yield of Hf K x rays (Fig. 2) and using a fluorescence yield $\omega_K = 0.955$ [13]. The normalized experimental spectrum was fit with a theoretical spectrum calculated using the code developed by Surić *et al.* and convoluted with the response function of the detector. The response shape was parametrized as the sum of a Gaussian peak, an exponential tail on the low energy side, Ge $K\alpha$ and $K\beta$ x-ray escape peaks, and a flat tail. (Over the limited fitting region of 70–97 keV a flat tail is quite adequate to

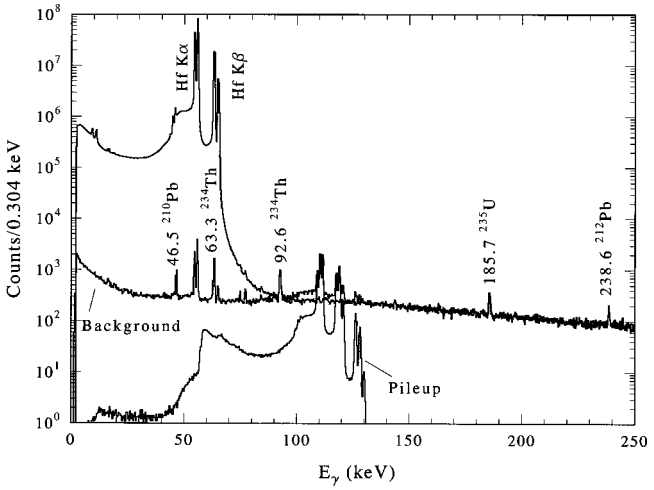

FIG. 3. The raw ''low count rate'' gamma-ray spectrum of ^{179}Ta, together with normalized background and pileup spectra. The ^{179}Ta spectrum represents 25.00 days of counting at an average count rate of 176.6 counts per second.

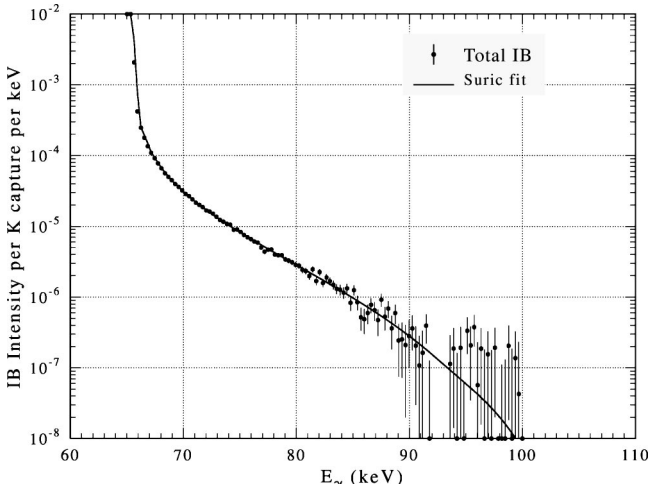

FIG. 4. Net IB spectrum of ^{179}Ta, obtained from the ''high count rate'' data. The solid line is a normalized fit using the calculation of Surić *et al.* Only data in the 70–97 keV energy region were used in the fit. The multiplicative factor for the theoretical calculation is 1.143 ± 0.014.

describe the Compton-scattered portion of the spectrum. For photons with energy of 97 keV or less the sharp backscatter edge is below 70 keV and hence falls below the fitted region.) Both the exponential tail and the flat tail were convoluted with a Gaussian that had the same width as the main Gaussian peak. The shape parameters were interpolated as a function of photopeak energy from the shape parameters obtained for the Hf K x rays and for the ^{133}Ba 53-keV and 81-keV lines and the ^{109}Cd 88-keV line. The variation of photopeak efficiency with energy was also obtained using the ^{133}Ba source, after correcting for summing effects. In calculating the theoretical IB yield the atomic binding energies (of Hf) which enter into the phase space factor were obtained from the tables of Larkins [14]. The wave functions which enter into the calculation of the energy-dependent IB matrix elements were obtained in the field of the daughter (Hf) atom, while the normalizing electronic wave function which determines the (nonradiative) K-capture rate was obtained in the field of the parent (Ta) atom.

Two parameters were allowed to vary freely in the fit: (1) a multiplicative normalization factor A and (2) the electron capture Q value Q_{EC}. Figure 4 shows the best fit to data in the 70–97 keV energy range. Data points in the vicinity of the 92.6-keV ^{234}Th background line were omitted from the fit. The resulting χ^2 per degree of freedom and the best fit parameters for both the ''high count rate'' and ''low count rate'' data are shown in Table I. The first error listed in the table is statistical and the second systematic. The latter was estimated from the change in the fitted parameters with reasonable variations in background, accidentals and pileup subtractions, the relative photopeak efficiency, and the shape parameters used in convoluting the theoretical IB spectrum. The results of the fits to the two data sets are in fair agreement with each other and indicate that possible systematic errors due to pileup and background subtractions are consistent with the quoted errors on the results.

Since the IB yield in the region just above the $K\alpha$ and $K\beta$ x rays is 4 to 5 orders of magnitude smaller than the yield of the x rays, just below, it is important to ascertain that the yield in the IB region is not due to the response function of the detector, i.e., that it is not due to an instrumental long term high energy tail of the x-ray peaks. It is very difficult to test the response function of the detector at that level in that energy region. All radioactive sources are accompanied by internal or external bremsstrahlung at a level comparable to that of ^{179}Ta. However, it is possible to verify that the yield in the IB region is due to higher energy γ rays, rather than the tail of lower energy x rays, by means of differential attenuation. To that end, we collected a ^{179}Ta spectrum with a 1.2 mm Cu absorber in front of the detector. The spectrum was collected for a period of 12.50 d at an average count rate of 38.70 cps. Figure 5 shows the ratio of counts from this spectrum, after background subtraction, to that of the ''high

TABLE I. Fitting results for total IB spectra.

	High count rate	Low count rate	Weighted average
Count rate	326.4 Hz	176.6 Hz	
Data points	84	84	
χ^2	71.81	86.44	
Q_{EC} (keV)	$105.03 \pm 0.39 \pm 0.25$	$106.11 \pm 0.57 \pm 0.25$	$105.37 \pm 0.32 \pm 0.25$
A	$1.143 \pm 0.014 \pm 0.025$	$1.111 \pm 0.018 \pm 0.025$	$1.131 \pm 0.011 \pm 0.025$

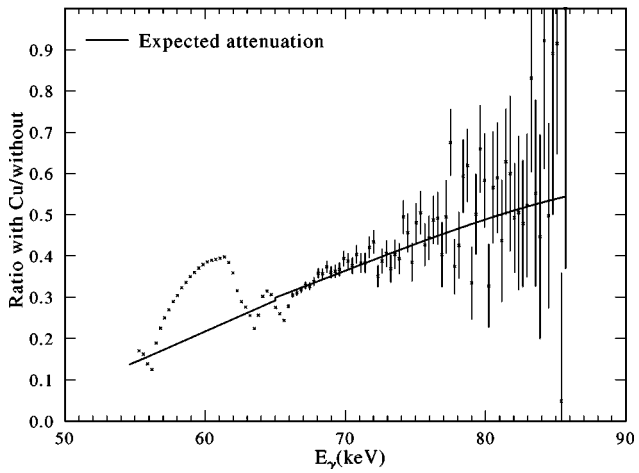

FIG. 5. The ratio of a net spectrum of ^{179}Ta taken with a Cu absorber of nominal thickness 1.2 mm to a net spectrum taken without the Cu absorber. The solid line is the expected ratio, calculated from tabulated attenuation coefficients.

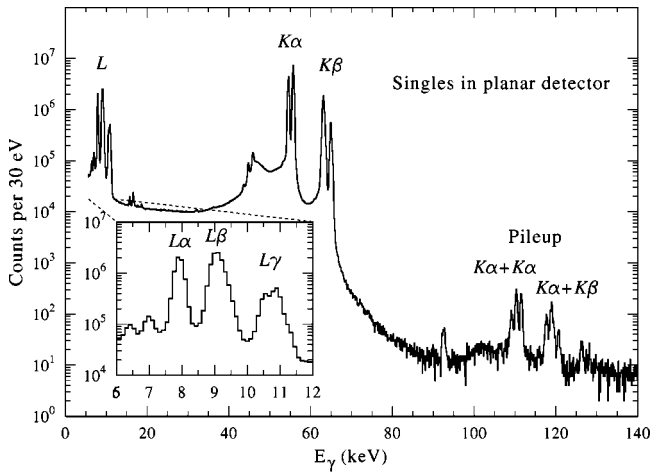

FIG. 6. A sample singles spectrum of the ^{179}Ta source, recorded with the planar Ge detector during the $2p$ IB measurements. The inset shows the region of the L x rays of Hf.

count rate'' run. The solid line shows the expected ratio, calculated from tabulated attenuation coefficients for gamma rays at the indicated energies. (The line represents an absolute calculation, not a fit to the measured ratio.) The relative decrease between the $K\alpha$ and $K\beta$ peaks was used to calculate an effective thickness for the Cu, to take into account variations due to angle of traversal through the Cu and possible thickness inhomogeneities. The resulting thickness of 1.19 mm is consistent with the nominal thickness of the Cu sheets which were used. With the effective thickness and measured ratio at the $K\alpha$ energy determined, the expected ratio at other energies could be calculated. From Fig. 5 it is clear, at least qualitatively, that the measured ratio in the IB region is consistent with the expected ratio; if a substantial portion of counts in the IB region were due to the high energy tail of the $K\alpha$ and/or $K\beta$ x rays, then the ratio in the IB region would have been comparable to the measured ratio for the $K\alpha$ and/or $K\beta$ x rays. (The increase in the ratio of counts between the two x ray lines is due to the increase in the low energy tail of the $K\beta$ x ray, arising from forward scattering in the Cu absorber.)

2. 2p IB spectrum

Figure 6 shows a singles spectrum recorded in the planar detector. The inset shows the region of the L x rays. There are three main groups of L x rays, labeled $L\alpha$, $L\beta$, and $L\gamma$. The $L\alpha$ group contains a mixture of lines from the L_2 and L_3 shells, with those from the L_3 dominating. The $L\beta$ group contains a mixture of lines from the L_1, L_2, and L_3 shells, with those from the L_2 dominating. The $L\gamma$ group contains a mixture of lines from the L_1 and L_2 shells, with those from the L_1 dominating. Because of absorption in the source, the efficiencies for the three different groups are not equal. Therefore a single gate on all the L x rays would not produce a correct $2p$ spectrum, but rather one weighted more heavily with contributions from the $2p_{1/2}$ subshell (because of the smaller absorption of the higher energy L x rays it produces). However, by obtaining two separate spectra, one gated on the $L\alpha$ group and the other on the $L\beta$ group, and obtaining the yield of the $K\alpha_1$ and $K\alpha_2$ x-ray lines in each of these spectra, one can solve for the $2p_{1/2}$ and $2p_{3/2}$ IB spectra and form a properly weighted total $2p$ IB spectrum. Specifically, let $dN(\mathrm{IB}\times L\alpha)$ be the experimentally measured yield of IB in some energy interval dE at energy E in coincidence with $L\alpha$ x rays. Then that yield can be related to the number of K captures (during the counting period), N_K, the efficiency for detecting IB photons at energy E in the IB detector $\epsilon_1(\mathrm{IB})$, the efficiency for detecting $L\alpha$ x rays in the x-ray detector $\epsilon_2(L\alpha)$, the IB yield from the L_2 shell per K capture in the energy interval dE $d\omega_2(\mathrm{IB})$ (convoluted with detector response), the corresponding IB yield from the L_3 shell $d\omega_3(\mathrm{IB})$, the number of $L\alpha$ x rays emitted per L_2 vacancy $n_{L_2L\alpha}$, and the number of $L\alpha$ x rays emitted per L_3 vacancy $n_{L_3L\alpha}$ by

$$dN(\mathrm{IB}\times L\alpha)=N_K\,\epsilon_1(\mathrm{IB})\,\epsilon_2(L\alpha)\,[d\omega_2(\mathrm{IB})\,n_{L_2L\alpha}+d\omega_3(\mathrm{IB})\,n_{L_3L\alpha}]. \quad (1)$$

Using similar notation, the yields $N(K\alpha_1\times L\alpha)$ and $N(K\alpha_2\times L\alpha)$ of $K\alpha_1$ and $K\alpha_2$ x rays in coincidence with $L\alpha$ x rays can be written as

$$N(K\alpha_1\times L\alpha)=N_K\,\epsilon_1(K\alpha)\,\epsilon_2(L\alpha)\,n_{KK\alpha_1}\,n_{L_3L\alpha}, \quad (2)$$

$$N(K\alpha_2\times L\alpha)=N_K\,\epsilon_1(K\alpha)\,\epsilon_2(L\alpha)\,n_{KK\alpha_2}\,n_{L_2L\alpha}, \quad (3)$$

where $n_{KK\alpha_i}$ is the number of $K\alpha_i$ x rays per K vacancy (these can be obtained from the tables given in Ref. [15]). In the above we have taken the efficiency for $K\alpha_1$ and $K\alpha_2$ x rays to be the same, which is a very good approximation for the larger coaxial Ge detector used for IB detection in the $2p$ coincidence experiments. Using Eqs. (2) and (3) to solve, respectively, for $n_{L_3L\alpha}$ and $n_{L_2L\alpha}$ and substituting the results into Eq. (1) we obtain

$$dN(\mathrm{IB}\times L\alpha)=\frac{\epsilon_1(\mathrm{IB})}{\epsilon_1(K\alpha)}\left[\left(\frac{N(K\alpha_2\times L\alpha)}{n_{KK\alpha_2}}\right)d\omega_2(\mathrm{IB})+\left(\frac{N(K\alpha_1\times L\alpha)}{n_{KK\alpha_1}}\right)d\omega_3(\mathrm{IB})\right]. \quad (4)$$

The above expression relates the two unknowns $d\omega_2(\mathrm{IB})$ and $d\omega_3(\mathrm{IB})$ to the experimentally measured coincidence yields and well-known atomic quantities ($n_{KK\alpha_i}$, with an uncertainty of 1% [15]), but which *does not* depend on the efficiency for detecting $L\alpha$ x rays, a quantity which is usually difficult to measure accurately because of the nonnegligible self-absorption in the source, or on $n_{L_iL\alpha}$, a quantity which has an estimated error of 5% [15]. One can similarly relate the measured yields of IB photons, $K\alpha_1$ x rays, and $K\alpha_2$ x rays in coincidence with $L\beta$ x rays to the unknowns $d\omega_2(\mathrm{IB})$ and $d\omega_3(\mathrm{IB})$ by

$$dN(\mathrm{IB}\times L\beta)=\frac{\epsilon_1(\mathrm{IB})}{\epsilon_1(K\alpha)}\left[\left(\frac{N(K\alpha_2\times L\beta)}{n_{KK\alpha_2}}\right)d\omega_2(\mathrm{IB})+\left(\frac{N(K\alpha_1\times L\beta)}{n_{KK\alpha_1}}\right)d\omega_3(\mathrm{IB})\right]. \quad (5)$$

One can then solve Eqs. (4) and (5) for the two unknowns $d\omega_2(\mathrm{IB})$ and $d\omega_3(\mathrm{IB})$ and obtain the proper sum $d\omega_2+d\omega_3$.

Figure 7 shows real and accidental spectra gated on the $L\alpha$ and $L\beta$ groups, from the 1996 set. A sample singles spectrum is also shown, for comparison. The pileup spectra in the figure were calculated as described in Ref. [11]. It should be mentioned that the pileup spectra were calculated assuming that the resolving time for pileup rejection is independent of the relative heights of the detector pulses. The fact that after subtraction of the pileup spectrum there was residual pileup of L and $K\alpha$ x rays (when, as mentioned previously, the Al absorber was not used) suggests that the resolving time is larger for a small pulse that follows a large pulse than for two pulses of comparable height. The number of residual $L+K\alpha$ pileup events observed when the Al absorber was not in place can be used to estimate the fraction of unsubtracted pileup events in that region of the IB spectrum. That fraction is about 1.5% for the planar detector and 0.5% for the coaxial detector. These fractions are considerably smaller than the statistical errors on the measured intensities of the $2p$ spectra and have been included in our estimate of the systematic errors (see below).

After subtracting the contributions of pileup and of accidental coincidences, the total $2p$ IB spectra were formed by solving Eqs. (4) and (5) at each energy bin and the resulting spectra fitted with the calculation of Surić *et al.*, over the energy interval 60–97 keV. The theoretical spectra were convoluted with the response function of the detector, measured with ^{109}Cd and ^{133}Ba calibration sources. There were two free parameters in the fit: (1) a multiplicative normalization factor A and (2) Q_{EC}. Figure 8 shows the data from the 1996 set, together with the best fit. Also shown, for comparison, are the total IB spectrum and its fit.

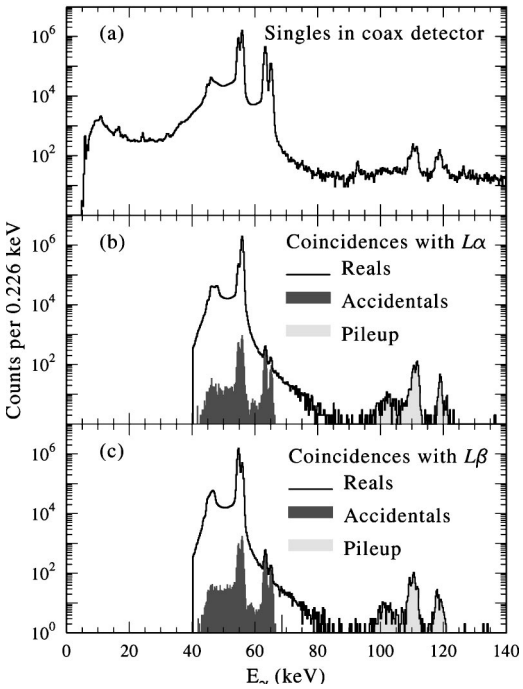

FIG. 7. (a) Sample singles spectrum recorded in the coaxial detector. (b) Spectrum recorded in the coaxial detector in true coincidence with $L\alpha$ x rays recorded in the planar detector. The accidental coincidence spectrum is shown as dark shaded. The light shaded spectrum is the simulated pileup spectrum. (c) Same as (b), but for coincidences with the $L\beta$ group.

Table II shows the results of the fits for the four different data sets, along with the weighted averages. The first error listed in the table is statistical and the second systematic. The latter was estimated from the change in the fitted parameters with reasonable variations in accidentals and pileup subtrac-

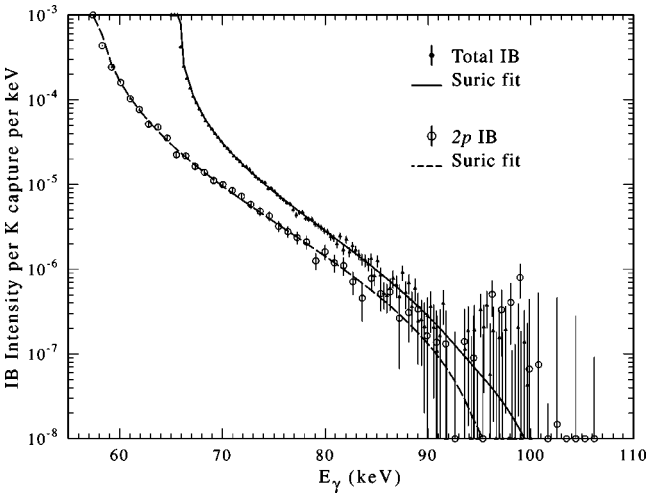

FIG. 8. Total and $2p$ IB spectra of ^{179}Ta, together with fits using the calculation of Surić *et al.* For the total spectrum the fitted region was 70–97 keV; for the $2p$ spectrum the fitted region was 60–97 keV.

TABLE II. Fitting results for $2p$ IB spectra.

Data set	IB detector	Al absorber	A	Q_{EC} (keV)
1996	Coaxial	Yes	$1.123\pm0.019\pm0.026$	$107.70\pm0.90\pm0.81$
1991	Coaxial	Yes	$1.040\pm0.035\pm0.026$	$108.90\pm2.09\pm0.81$
1991	Coaxial	No	$1.090\pm0.109\pm0.026$	$108.16\pm2.68\pm0.81$
1991	Planar	No	$1.067\pm0.034\pm0.026$	$103.82\pm1.52\pm0.81$
Weighted average			$1.097\pm0.015\pm0.026$	$107.04\pm0.70\pm0.81$
Total IB	Planar	Yes	$1.131\pm0.011\pm0.025$	$105.37\pm0.32\pm0.25$

tions, the relative photopeak efficiency, the shape parameters used in convoluting the theoretical IB spectrum, and the limits of the fitting range. We also tested the stability of the fitted parameters with changes in the binning size; the reason for such a test is that near the end point (in the $2p$ coincidence spectrum) the statistics are low and hence the errors may be non Gaussian, while the χ^2 test assumes Gaussian errors. We indeed found that the bin width of ≈ 0.225 keV (which was close to the bin width of 0.304 keV used with the total IB spectra, measured in singles) was too small when used with the $2p$ coincidence spectra; i.e., when a larger bin width was used, the fitting results did change by an amount approximately equal to the statistical error. Therefore we kept doubling the bin width until the fitted parameters did not change when using the next doubled bin width; as a result, the bin width used in the $2p$ coincidence spectrum was 0.903 keV. The adequacy of the use of χ^2 fitting with such a bin width was also confirmed by fitting Monte Carlo–generated spectra (with statistics comparable to those of the experimental data). The fits gave back the Q value and normalization parameter used in generating the spectra when the bin width was 0.903 keV, but gave results with deviations similar to those observed for the experimental data when the smaller bin width of 0.225 keV was used.

The normalization parameters for the $2p$ and total IB spectra differ by only $3.4\pm3.1\%$. The closeness of the values of these normalization parameters suggests that the calculation of Surić *et al.* reproduces the relative intensities of the IB spectra from the different shells very well. Note that one cannot obtain an IB spectrum from the $3p$ and higher shells by simply subtracting the measured $2p$ spectrum from the measured total spectrum, because the two spectra were obtained with two different detectors, having different response functions and different relative efficiencies. There is a slight disagreement in the Q values extracted from the $2p$ and total IB spectra, but the disagreement is about 1.4 standard deviations (where we have combined all the errors in quadrature) and is not cause for serious concern. To test the effect of the Q value on the normalization parameter, we conducted fits on the $2p$ IB spectra with the Q value fixed at 105.37 keV, the value obtained from the total IB spectrum. The weighted average normalization in that case was $1.127\pm0.010\pm0.026$, a value which is in even better agreement with the normalization parameter of the total spectrum.

B. *L*-to-*K* capture ratio measurements

Figure 9 shows the spectrum of L x rays recorded in the planar Ge detector in coincidence with $K\alpha$ x rays recorded in the well-type NaI detector (solid line), superimposed on the L x-ray spectrum recorded in anticoincidence (dotted line). The locations of the major lines arising from vacancies in the L_1, L_2, and L_3 subshells are also shown. The Q_{EC} was deduced from an analysis of these spectra as follows. The yield $N(L\alpha\times K\alpha)$ of $L\alpha(=L\alpha_1+L\alpha_2)$ x rays in coincidence with $K\alpha$ x rays is given by

$$
\begin{aligned}
N(L\alpha\times K\alpha) &= NP_K \\
&\times \omega_K\left[\frac{K\alpha_1}{K}+\frac{K\alpha_2}{K}f_{23}+\frac{K\alpha_3}{K}(f_{13}+f'_{13}+f_{12}f_{23})\right] \\
&\times \omega_3\frac{L\alpha}{L_3} \\
&\times \epsilon_{\mathrm{Ge}}(L\alpha)\,\epsilon_{\mathrm{NaI}}(K\alpha), \qquad (6)
\end{aligned}
$$

where N is the number of decays, P_K is the probability of K capture per decay, ω_K is the fluorescence yield of the K shell,

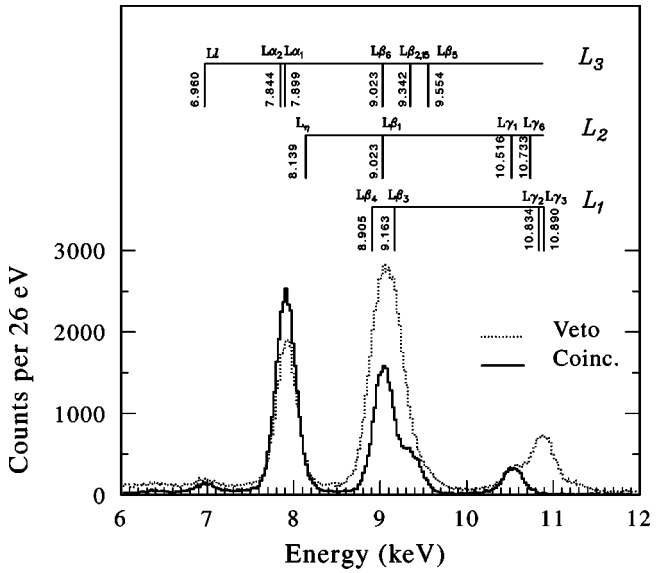

FIG. 9. L x-ray spectra recorded in the planar Ge detector in coincidence with (solid line) and in anticoincidence (dotted line) with $K\alpha$ x rays. The labels give the energy (in keV) and vacancy from which each line originates.

$K\alpha_i/K, i=1,2,3$ are the K x-ray branching ratios for transitions to the L_3, L_2, and L_1 shells, respectively (here we refer to the upward transition of a vacancy), ω_3 is the fluorescence yield of the L_3 shell, $L\alpha/L_3$ is the branching ratio of the $L\alpha$ x-ray line, f_{ik} is the Coster-Kronig yield for radiationless transitions between the L_i and L_k levels, f'_{13} is the intrashell radiative yield for the transition $L_1 \rightarrow L_3$, $\epsilon_{\mathrm{Ge}}(L\alpha)$ is the photopeak efficiency of the planar Ge detector for detecting $L\alpha$ x rays, and $\epsilon_{\mathrm{NaI}}(K\alpha)$ is the photopeak efficiency of the NaI detector for detecting $K\alpha$ x rays. [Figure 1 shows a schematic of the setup used in these measurements and Fig. 10 shows the atomic transitions referred to in Eq. (6).] The first line in the above equation gives the number of K vacancies produced (thus leading to the possibility of observing a $K\alpha$ x ray), the second line gives the probability that the K vacancy produces a $K\alpha$ x ray *and* a vacancy in the L_3 subshell (thus leading to the possibility of observing a coincident $L\alpha$ x ray), the third line gives the probability that an $L\alpha$ x ray is emitted in filling the L_3 vacancy, and the fourth line gives the probability that the emitted $K\alpha$ and $L\alpha$ are detected (at full energy) in their respective detectors. In the second line, the first term in square brackets accounts for the radiative transition from the K shell directly to the L_3 subshell, the second term $[(K\alpha_2/K)f_{23}]$ accounts for the production of the L_3 vacancy by first having a radiative transition from the K shell to the L_2 subshell, followed by a Coster-Kronig transition (with probability f_{23}) from the L_2 subshell to the L_3 subshell, and the last term accounts for the production of the L_3 vacancy by first having a radiative transition from the K shell to the L_1 subshell (with the admittedly small branching ratio $K\alpha_3/K$), followed by either a radiative transition from L_1 to L_3 (with probability f_{13}), or a radiative transition (with probability f'_{13}), or a sequence of Coster-Kronig transitions $L_1 \rightarrow L_2 \rightarrow L_3$ (with probability $f_{12}f_{23}$).

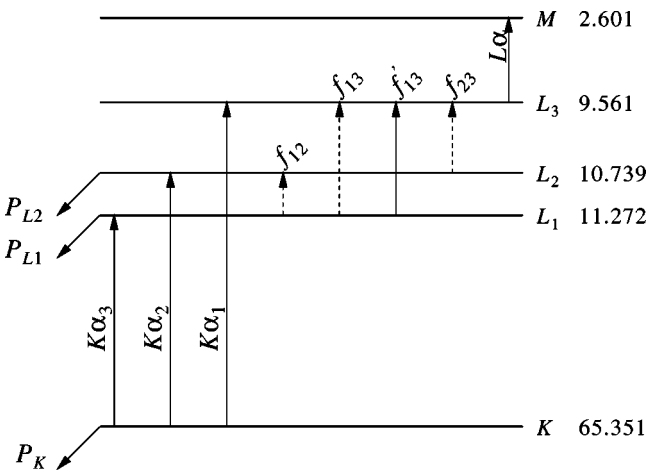

FIG. 10. Atomic level diagram (not to scale) showing most of the transitions and intensities referred to in Eqs. (6) and (7). The diagonal arrows indicate the capture of an electron from the corresponding atomic orbital. Upward arrows show the transfer of a vacancy from a deeper to a shallower atomic level via a radiative transition (solid line) or a nonradiative transition (dashed line). The indicated binding energies are those in the daughter atom Hf, in keV.

The yield $N(L\alpha \times \overline{K\alpha})$ of $L\alpha$ x rays in anticoincidence with $K\alpha$ x rays is given by

$$
\begin{aligned}
N(L\alpha \times \overline{K\alpha}) = N\,\omega_3 \frac{L\alpha}{L_3}\epsilon_{\mathrm{Ge}}(L\alpha) \\
\times [P_{L_1}(f_{13}+f'_{13}+f_{12}f_{23}) \\
+ P_{L_2} f_{23} \\
+ P_K(f_{KL_3}+f'_{KL_3}\{1-[\eta_{\mathrm{NaI}}(K\alpha)+\eta_{\mathrm{Ge}}(K\alpha)-\eta_{\mathrm{Ge,NaI}}(K\alpha)]\})],
\end{aligned}
\tag{7}
$$

where P_{L_i} is the probability of electron capture (per decay) from subshell L_i, f_{KL_3} is the radiationless yield of L_3 vacancies per K vacancy (due to Auger transitions of a K-shell vacancy), and f'_{KL_3} the radiative yield of L_3 vacancies per K vacancy, $\eta_{\mathrm{NaI}}(K\alpha)$ and $\eta_{\mathrm{Ge}}(K\alpha)$ are the total efficiencies of the NaI and Ge detectors, respectively, for detecting $K\alpha$ x rays, and $\eta_{\mathrm{Ge,NaI}}(K\alpha)$ is the probability that a $K\alpha$ x ray leaves a signal in both the Ge and NaI detectors (through Compton scattering from one detector to the other and through I x-ray escape from the NaI to the Ge detector).

In Eq. (7) the term on the second line accounts for the production of L_3 vacancies by L_1 capture (with probability P_{L_1}) followed by a transfer of the L_1 vacancy to the L_3 shell by a radiationless transition (with yield f_{13}) or a radiative transition (with yield f'_{13}), or a sequence of radiationless transitions $L_1 \rightarrow L_2 \rightarrow L_3$ (with probability $f_{12}f_{23}$). The term in the third line accounts for the production of L_3 vacancies by L_2 capture (with probability P_{L_2}) followed by a transfer of the L_2 vacancy to the L_3 shell by a radiationless transition (with yield f_{23}). (Direct capture from the L_3 shell is forbidden.) Clearly capture from the L_1 and L_2 shells does not produce $K\alpha$ x rays and hence the resulting $L\alpha$ x rays will be a subset of those in anticoincidence with $K\alpha$ x rays. The term on the fourth line accounts for the production of L_3 vacancies by K capture (with probability P_K), followed by a radiationless (Auger) transition of the vacancy from the K

shell to the L_3 shell (with yield f_{KL_3}) or a radiative transition (with yield f'_{KL_3}), provided the emitted $K\alpha$ x ray is not detected (i.e., is in anticoincidence with the $L\alpha$ x ray). The probability that the $K\alpha$ x ray is not detected is 1 minus its probability of being detected either in the NaI detector $[\eta_{\mathrm{NaI}}(K\alpha)]$ or the Ge detector $[\eta_{\mathrm{Ge}}(K\alpha)]$ (the reason that detection in the Ge detector leads to vetoing is that the $K\alpha$ signal sums with the $L\alpha$ signal, thus throwing the $L\alpha$ signal out of its photopeak region); however, both $\eta_{\mathrm{NaI}}(K\alpha)$ and $\eta_{\mathrm{Ge}}(K\alpha)$ (being *total* efficiencies) contain the same contribution $\eta_{\mathrm{Ge,NaI}}(K\alpha)$ of events in which the $K\alpha$ leaves a signal in both detectors and hence that contribution is doubly counted in the sum $\eta_{\mathrm{NaI}}(K\alpha)+\eta_{\mathrm{Ge}}(K\alpha)$ and should be subtracted away once to form the correct vetoing probability. [The above is simply a restatement of the elementary probability theory result $P(A \text{ or } B)=P(A)+P(B)-P(A \text{ and } B)$.]

The radiative yield of L_3 vacancies per K vacancy was calculated as in Eq. (6), namely,

$$f'_{KL_3}=\omega_K\left[\frac{K\alpha_1}{K}+\frac{K\alpha_2}{K}f_{23}+\frac{K\alpha_3}{K}(f_{13}+f'_{13}+f_{12}f_{23})\right]. \tag{8}$$

The radiationless yield f_{KL_3} was calculated as the number of L_3 vacancies per K vacancy minus the radiative yield f'_{KL_3}:

$$f_{KL_3}=\frac{n_{KL\alpha_1}}{n_{L_3L\alpha_1}}-f'_{KL_3}. \tag{9}$$

As can be seen, the number of L_3 vacancies per K vacancy was calculated from the ratio of the number of $L\alpha_1$ x rays per K vacancy ($n_{KL\alpha_1}$) to the number of $L\alpha_1$ x rays per L_3 vacancy ($n_{L_3L\alpha_1}$).

Expressions similar to those given in Eqs. (6) and (7) were obtained for the yields of $L\beta$ and $L\gamma$ x rays in coincidence and in anticoincidence with $K\alpha$ x rays. In those expressions the radiationless yield f_{KL_i} and radiative yield f'_{KL_i} of L_i vacancies per K vacancy were calculated using expressions similar to those given in Eqs. (9) and (8), respectively.

For the allowed decay of ^{179}Ta the capture fractions are related to the Q_{EC} value by [1]

$$P_i=C\,\beta_i^2\,B_i(Q_{\mathrm{EC}}-E_i)^2, \tag{10}$$

where C contains the nuclear matrix element, β_i is the Coulomb amplitude of the bound-state electron radial wave function in orbital i, B_i is the associated electron exchange and overlap correction, and E_i is the electron binding energy in the daughter (Hf) atom.

By dividing Eq. (7) by Eq. (6) one can eliminate N and $\epsilon_{\mathrm{Ge}}(L\alpha)$ [and in the corresponding equations for $L\beta$ and $L\gamma$ eliminate $\epsilon_{\mathrm{Ge}}(L\beta)$ and $\epsilon_{\mathrm{Ge}}(L\gamma)$] and solve for Q_{EC} using the experimentally measured yields $N(L\alpha\times K\alpha)$ and $N(L\alpha\times\overline{K\alpha})$, the experimentally measured efficiencies $\epsilon_{\mathrm{NaI}}(K\alpha)$, $\eta_{\mathrm{NaI}}(K\alpha)$, $\eta_{\mathrm{Ge}}(K\alpha)$, and $\eta_{\mathrm{Ge,NaI}}(K\alpha)$, and the tabulated atomic quantities (ω_K, f_{ij}, . . .). We emphasize again that our technique enables us to measure Q_{EC} without having to know the L x-ray efficiency, a quantity which is usually difficult to measure accurately because of the non-negligible self-absorption in the source. Although the $L\beta$ group contains peaks from different shells, these are sufficiently close in energy to be characterized by a single efficiency $\epsilon_{\mathrm{Ge}}(L\beta)$ that enters both the expressions for $N(L\beta\times K\alpha)$ and $N(L\beta\times\overline{K\alpha})$ as a multiplicative factor and hence cancels out in the ratio $N(L\beta\times\overline{K\alpha})/N(L\beta\times K\alpha)$. The same is true for the $L\gamma$ group. Another advantage to our method is the enhanced sensitivity to Q_{EC} that the anticoincidence with $K\alpha$ brings. Without anticoincidence [i.e., in a singles measurement of $N(L\alpha)$] the coefficient of P_K in Eq. (7) would be 0.538, while with anticoincidence the coefficient is only 0.101 (because of the large anticoincidence efficiency of the well-type NaI detector of 0.83). Thus the anticoincidence enhances the sensitivity of $N(L\alpha\times\overline{K\alpha})$ to P_{L_1} which in turn enhances the sensitivity to Q_{EC}.

TABLE III. Q_{EC} (keV) determined from L-to-K capture ratios.

Source	Peak $L\alpha$	$L\beta$	$L\gamma$
1990	110.8±4.3	108.9±4.6	107.5±6.7
1992	111.6±4.7	110.4±4.7	106.6±6.4
Overall average	109.3±3.1		

The various efficiencies for the $K\alpha$ x rays were obtained from a knowledge of the absolute emission rates of these x rays by the ^{179}Ta sources. That emission rate was measured by first obtaining an efficiency curve for the Ge detector using calibrated sources of ^{133}Ba, ^{109}Cd, and ^{57}Co placed at a distance of 13.1 cm from the face of the detector; this distance is large enough that summing effects could be ignored. In all the efficiency measurements a precision pulser was used to correct for (the usually small) dead time. The various atomic quantities that enter into Eqs. (6)–(10) (and their equivalents for the $L\beta$ and $L\gamma$ peaks) were obtained from the tables given in Ref. [15] and from Refs. [13,16]. Table III lists the Q_{EC} values deduced from each of the L x-ray peaks for the two ^{179}Ta sources. All the results agree within their stated errors. The unweighted average for the Q_{EC} value deduced from these L to K capture ratio measurements is 109.3±3.1 keV. The error in the average takes proper account of the correlation between the errors on the individual Q's because of their common dependence on the same atomic quantities. In fact, the errors in the atomic quantities dominate the errors in all the Q's. These errors are dominated, in turn, by the errors on ω_1 (15%), ω_2 (5%), ω_3 (5%), f_{12} (20%), f_{13} (10%), and f_{23} (15%) [13]. While it is likely that the errors on these atomic yields are correlated, it is nearly impossible for us to determine what these correlations may be, since the atomic yields were derived from many sources [13]; therefore we have simply combined the errors on the above atomic yields in a statistical way.

IV. DISCUSSION AND CONCLUSIONS

The measured normalization parameters of $A=1.131\pm0.027$ for the total IB spectrum and $A=1.097\pm0.030$ for

the $2p$ IB partial spectrum (where, for simplicity, we have combined the statistical and systematic errors in quadrature) suggest that the calculation of Surić *et al.* does underestimate the IB yield. While this underestimation does seem to grow with Z (from $7.0\pm2.4\%$ for ^{139}Ce [$Z=58$] to $13.1\pm2.7\%$ for ^{179}Ta [$Z=73$]), it is substantially less than the factor of 1.5–2 observed for ^{193}Pt ($Z=78$). Thus, the large discrepancy observed for ^{193}Pt remains somewhat of a puzzle. Perhaps the treatment of the decay as an allowed decay, even though it is first-forbidden nonunique, is not valid. A confirmation of the measured intensity for ^{193}Pt might be desirable.

The discrepancy of 10–13 % between the intensity predicted by the calculation of Surić *et al.* and the current measurement, while relatively small, is, nevertheless, statistically significant. The origin of this discrepancy is not obvious to us. Possible improvements to the calculation of Surić *et al.* which could be made within the context of the independent-particle approximation are (1) inclusion of exchange-overlap corrections and (2) taking into account the different Z dependences of the two time orders in the electron propagator, namely, the fact that radiation before capture occurs in the field of element Z, while radiation after capture takes place in the field of element $Z-1$ [17]. Both of these effects have been considered before by Persson and Koonin [17,18], but at much lower Z and higher Q_0, where the IB spectra are dominated by $1s$ and (to a lesser extent) $2s$ capture. At some stage true many-body effects in the atomic wave functions may have to be taken into account, as well, but these are obviously outside the scope of the independent-particle approximation of Surić *et al.*

The Q_{EC} value of 109.3 ± 3.1 extracted from the L-to-K capture measurements is in fair agreement with the Q_{EC} value of 105.61 ± 0.41 extracted from IB end-point measurements (where we have taken the weighted average of the values extracted from the total and $2p$ IB spectra and, for simplicity, combined the statistical and systematic errors in quadrature). Two old and mildly discrepant values of Q_{EC} exist, that of Bisi *et al.* (103 ± 6 keV [19]) and that of Jopson *et al.* (121 ± 7 keV [20]),[1] while the mass tabulations give $Q_{EC}=110\pm5$ keV [21]. Because of the substantially larger error of the Q values determined from L-to-K capture measurements (compared to those determined from the IB end-point energy), it is not possible to use those to confirm the validity of the extrapolated shape used in the IB fit (recall that the fitting region we use ends about 8 keV below the extracted Q value). The dominant error in the Q value we determined from the L-to-K capture measurements is the uncertainty in the values of the L_1 subshell fluorescence (ω_1) and Coster-Kronig (f_{12} and f_{13}) yields. (If the error in the atomic quantities were ignored, the resulting error in the Q value would be 1.7 keV.) It should be possible to improve on these values by conducting measurements which make use of one of the existing synchrotron radiation facilities. In such a measurement the number of L_1 vacancies that is created could be measured by detecting the emitted photoelectrons; ω_1, f_{12}, and f_{13} could be measured by detecting the number of L x rays originating in the L_1, L_2, and L_3, respectively, in coincidence with the photoelectrons.

ACKNOWLEDGMENTS

The assistance of James Parker in collecting data is gratefully acknowledged. This work was supported by U.S. DOE Grant Nos. DE-FG05-87ER40314, DE-FG02-96ER40955, and DE-AC03-76F00098.

[1]We have recalculated the Q values of these references based on their published L-to-K yields, but using current values of fluorescence and Coster-Kronig yields.

[1] W. Bambynek, H. Behrens, M. H. Chen, B. Crasemann, M. L. Fitzpatrick, K. W. D. Ledingham, H. Genz, M. Mutterer, and R. L. Intemann, Rev. Mod. Phys. **49**, 77 (1977).
[2] A. De Rújula, Nucl. Phys. **B188**, 414 (1981).
[3] K. Riisager, A. De Rújula, P. G. Hansen, B. Jonson, and H. L. Ravn, Phys. Scr. **31**, 321 (1985).
[4] R. J. Glauber and P. C. Martin, Phys. Rev. **104**, 158 (1956).
[5] P. C. Martin and R. J. Glauber, Phys. Rev. **109**, 1307 (1958).
[6] P. T. Springer, C. L. Bennett, and P. A. Baisden, Phys. Rev. A **35**, 679 (1987).
[7] Particle Data Group, L. Montanet *et al.*, Phys. Rev. D **50**, 1173 (1994).
[8] T. Surić, R. Horvat, and K. Pisk, Phys. Rev. C **47**, 47 (1993).
[9] M. M. Hindi, R. L. Kozub, and S. J. Robinson, Phys. Rev. C **49**, 3289 (1994).
[10] M. M. Hindi, R. L. Kozub, and S. J. Robinson, Phys. Rev. C **52**, 2780 (1995).
[11] M. M. Hindi and R. L. Kozub, Phys. Rev. C **54**, 2709 (1996).
[12] M. M. Hindi and R. L. Kozub, Phys. Rev. C **43**, 461 (1991).
[13] M. O. Krause, J. Phys. Chem. Ref. Data **8**, 307 (1979).
[14] F. B. Larkins, At. Data Nucl. Data Tables **20**, 313 (1977).
[15] *Table of Radioactive Isotopes*, edited by E. Browne, R. B. Firestone, and V. S. Shirley (Wiley, New York, 1986).
[16] S. I. Salem, S. L. Panossian, and R. A. Krause, At. Data Nucl. Data Tables **14**, 91 (1974).
[17] B. I. Persson and S. E. Koonin, Phys. Rev. C **5**, 1443 (1972).
[18] S. E. Koonin and B. I. Persson, Phys. Rev. C **6**, 1713 (1972).
[19] A. Bisi, L. Zappa, and E. Zimmer, Nuovo Cimento **4**, 307 (1956).
[20] R. C. Jopson, H. Mark, C. S. Swift, and J. H. Zenger, Phys. Rev. **124**, 157 (1961).
[21] A. H. Wapstra and G. Audi, Nucl. Phys. **A432**, 1 (1985).